Localized removal of layers of metal, polymer, or biomaterial by ultrasound cavitation bubbles

Rivas, David Fernandez; Verhaagen, Bram; Seddon, James R. T.; Zijlstra, Aaldert G.; Jiang, Lei-Meng; van der Sluis, Luc W. M.; Versluis, Michel; Lohse, Detlef; Gardeniers, Han J. G. E.

Published in:
Biomicrofluidics

DOI:
10.1063/1.4747166

Publication date:
2012

Localized removal of layers of metal, polymer, or biomaterial by ultrasound cavitation bubbles

David Fernandez Rivas,[1,a)] Bram Verhaagen,[2] James R. T. Seddon,[2] Aaldert G. Zijlstra,[2] Lei-Meng Jiang,[3] Luc W. M. van der Sluis,[3] Michel Versluis,[2] Detlef Lohse,[2] and Han J. G. E. Gardeniers[1]
[1]*Mesoscale Chemical Systems Group, MESA+ Research Institute, University of Twente, ME147, P.O. Box 217, 7500AE Enschede, The Netherlands*
[2]*Physics of Fluids Group, MIRA and MESA+ Research Institutes, Faculty of Science and Technology, University of Twente, P.O. Box 217, 7500AE Enschede, The Netherlands*
[3]*Department of Cario-, Endo- and Periodontology, Academic Center for Dentistry, Amsterdam, The Netherlands*

(Received 21 May 2012; accepted 6 August 2012; published online 21 August 2012)

We present an ultrasonic device with the ability to locally remove deposited layers from a glass slide in a controlled and rapid manner. The cleaning takes place as the result of cavitating bubbles near the deposited layers and not due to acoustic streaming. The bubbles are ejected from air-filled cavities micromachined in a silicon surface, which, when vibrated ultrasonically at a frequency of 200 kHz, generate a stream of bubbles that travel to the layer deposited on an opposing glass slide. Depending on the pressure amplitude, the bubble clouds ejected from the micropits attain different shapes as a result of complex bubble interaction forces, leading to distinct shapes of the cleaned areas. We have determined the removal rates for several inorganic and organic materials and obtained an improved efficiency in cleaning when compared to conventional cleaning equipment. We also provide values of the force the bubbles are able to exert on an atomic force microscope tip. © *2012 American Institute of Physics*. [http://dx.doi.org/10.1063/1.4747166]

I. INTRODUCTION

Bubbles have been under analysis at least since the Greek times,[1] and play an important role in physics, chemistry, medicine, and technology. The generation of bubbles by acoustic cavitation has been studied for many years, however, without special measures there is little control over its occurrence and their behavior can at first sight be surprising and puzzling.[2] Whether or not cavitation due to pressure oscillations will occur, depends not only on the acoustic field but also on physical properties and conditions such as the amount of gas in the liquid and the presence of nucleation sites. Once these are controlled, one can achieve fully controllable cavitation, in excellent agreement with the theoretical predictions.[3]

Cavitation has found use in several applications, based either on its chemical or on its mechanical effects.[4–7] In water solutions exposed to ultrasound, for example, an enhancement of chemical reactions can be achieved. Short lived radicals form at the breakdown of water molecules, due to the high pressures and temperatures in the collapsing bubble's interior.[8–10]

The use of acoustics in microfluidics and specially in bio-applications has received considerable attention in the last decade.[11–13] Acoustic cavitation can produce surface modifications, including damage, through high-speed liquids jets and shockwaves generated upon the asymmetric collapse of cavitation bubbles near a surface.[14–16] These mechanical effects have been considered by many as negative, as it may give rise to significant erosion and abrasion, for

[a)]Electronic mail: d.fernandezrivas@utwente.nl. Telephone: +31 53 489 2594.

example, demonstrated by the cavitation damage on ship propellers[2] and artificial heart valves.[17,18] However, in specific cases, the mechanical effect of cavitation has been shown to be useful for practical applications, for example, for cell disruption and drug uptake,[19,20] or mixing and particle size reduction,[21] besides several other biological effects.[15,22] Also in electronics, cavitation has been useful for the modification of surfaces (roughening, cleaning, and gold plating, among others), using liquids as benign as water. The undesired use of hazardous substances, high temperature, and long process times can be avoided or reduced by the use of cavitation.[23] The use of ultrasound has therefore been considered as a "green solution" for the above mentioned applications, given the reduction in power usage and chemicals.

Nevertheless, practical uses of cavitation are in general limited because of a lack of control over the location and amount of cavitation. Under the irradiation of ultrasound to a liquid, bubbles originate from nuclei at random locations. Quantification of cavitation effects (erosion and cleaning particularly) is very difficult due to its random occurrence and also due to different materials and equipment used in different laboratories and industrial equipment.[4,24] This situation has prevented the upscaling and extended usage of desirable effects of cavitation such as localized cleaning or surface modifications.[25] Control over cavitation location requires special measures as, for example, the use of a laser,[19] by seeding the liquid with particles and irradiating with a shockwave,[26] or from gas-filled crevices in smooth surfaces exposed to shockwaves,[27] or continuous ultrasonic irradiation.[28]

Here, we show the generation of cavitation in various liquids for fast removal (order of tenths of seconds) of several deposited materials from a glass substrate with millimetric control, based on well-defined cavitation nucleation sites.[28] This article will start with the description of the experimental setup for the localized generation of cavitation, as well as the methods for characterization of unwanted cavitation erosion on the underlying substrate. Next, a short description of the various materials that have been investigated for removal by cavitation is given. Additionally, to obtain information on the force generated by a bubble, a measurement of the magnitude of the forces that the bubbles exert on an atomic force microscope (AFM) tip is provided. The measured material removal rates will be presented and discussed; determination of the adhesion strength of the different materials is described in Appendices.

II. EXPERIMENTAL SETUP

A. Materials to be removed

The cleaning of surfaces is a process that is required in a wide variety of applications, with an equally wide range of materials that need to be removed from the given surface. Each of these materials and surfaces have their specific mechanical and chemical properties that provide different adhesion strengths between both. Here, we list some typical materials to be removed, which are all studied in this work.

1. Solid hard materials

The solid hard materials used in this study are gold (Au), platinum (Pt), chromium (Cr), and titanium (Ti), all categorized as metals, and Olin and AZ96, which can be categorized as organic materials, and are commonly used as photoresists in microfabrication of semiconductors and microelectromechanical systems (MEMS).

2. Soft biomaterials

Contrary to the solid hard materials, soft biological materials may deform (visco)elastically before cohesive or adhesive failure takes place.[29,30] Elastic materials typically display significant strain when subjected to a stress, and relax back to the initial shape and position when the stress is removed. Only when the stress exceeds the material's yield stress and enters the plastic domain of the soft material, cohesive failure will take place. Viscoelastic materials, however, exhibit viscous behavior when the stress exceeds the yield stress; the material will flow away and there will be a net displacement when the stress is removed.[31,32] One of the most

commonly encountered viscoelastic materials is the biofilm, which can often be found in pipes, on medical implants and inside and on teeth, where it often has a negative influence on efficiency or health.[30,33] The biofilm is a structure of bacteria enclosed by a self-produced extracellular matrix.[34,35] This matrix provides the viscoelastic properties of the biofilm, which protects the embedded bacteria from high stresses.

3. Cells

Another biological material of great importance nowadays is a cancer cell. The study of the reaction of a cell to different environmental conditions with minimal interference in their habitat is still a problem. Cavitation has been used to address this issue,[22,36] while it also is able to porate cells for drug uptake due to shear forces.[19]

B. Material removal experiments

1. Ultrasonic cavitation setup

The continuous and localized generation of acoustic cavitation bubbles has been accomplished by ultrasonically vibrating a silicon surface containing micropits.[28] When pouring liquid over the silicon substrate, individual gas bubbles were entrapped in the pits; vibrating the surface ultrasonically resulted not only in acoustic streaming from the oscillating surface, but for large enough pressures also in pinch-off of gas bubbles from the micropits, as detailed elsewhere.[37]

The silicon substrate with micropits was placed in a cavitation cell container made of glass with 25 mm outer diameter, 15 mm inner diameter, and 6 mm depth, matching one quarter of the wavelength at the operation frequency of 200 ± 5 kHz. A piezo element (PZ27, Ferroperm) of thickness 6 mm and diameter 25 mm was glued to the cell bottom. A sketch of the cavitation cell is given in Figure 1. For each experiment, the cell was filled with fresh ultra-pure water (milliQ, milliPore). Also, ethanol, bleach, and acetone were investigated given their extensive use in general and ultrasonic cleaning applications. Additionally, a cell cultivation liquid medium was used.

The micropits were etched under clean room conditions on double-side polished silicon wafers by means of a plasma dry-etching machine (Adixen AMS 100 SE, Alcatel). The wafer was then diced in square chips with a side of 10 mm. The edge of these substrates has a step of 58 μm with four notches radially and equally spaced (see Figure 2).

Each pit had a diameter of 30 μm and a depth of approximately 10 μm; multiple pits were arranged in four different configurations: single pits, two pits separated by a distance of 1 mm, three pits arranged at the corners of an equilateral triangle with a side of 1 mm, and four pits at the corners of a 1 mm side square.

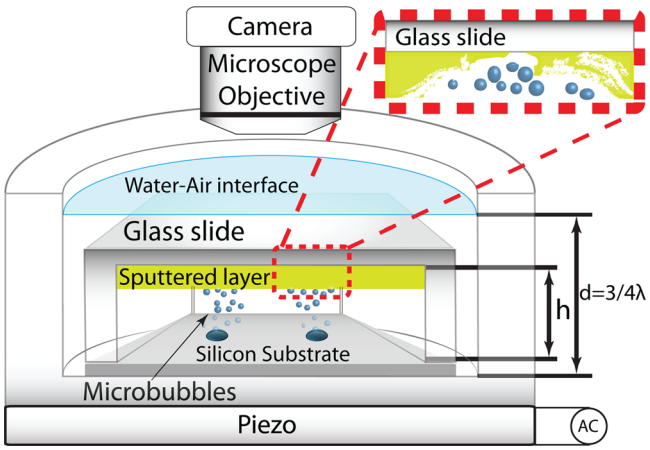

FIG. 1. Schematic representation of the experimental setup. The gap between the glass slide and the silicon substrate h = 100 μm. The water column height is 5 mm.

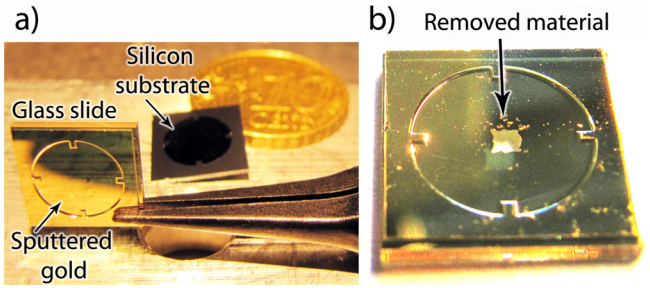

FIG. 2. (a) A black tweezer holds a gold sputtered glass slide prior to exposure to cavitating bubbles; in the background a silicon substrate is shown. (b) A zoomed view of the same glass slide after exposure to cavitating bubbles from four pits in the cavitation cell described in this paper. The glass slide has sides of 10 mm.

The piezo element was driven by a sinusoidal signal generated by an arbitrary waveform generator (33120 A, Hewlett Packard) and amplified by means of an audio amplifier (TA-FB740R QS, Sony). The voltage, current, and power to the piezo element were monitored with a power meter (HM8115-2, Hameg). The duration of the experiments was short enough (typically less than 5 min) so that the temperature increased no more than approximately 5 °C (measured with a T-type thermocouple with digital read-out; HI 93552 R, HANNA Instruments).

Two different power settings were used with all pit arrangements: Low (0.182 W) and high (0.629 W). The corresponding approximate acoustic pressure amplitudes were measured to be 225 kPa and 350 kPa, with error values provided by the manufacturer as 20%. These pressures were measured using a needle hydrophone (HNR-500, Onda) positioned 65 μm above the center of the chip.[41]

2. Imaging setup

The occurrence of cavitation and the removal of the deposited materials was imaged through the air-water interface with a CCD camera (LM165M, Lumenera Corp., Ottawa, ON, Canada), recording at a frame rate of 15 fps and an exposure time of 10 μs. For the removal of metal layers, a color high-speed camera (SA2, Photron, San Diego, CA, USA) was used, recording at frame rates between 60 and 2000 frames per second and an exposure time of 30 μs. The cameras were attached to a microscope (BX-FM, Olympus, Tokyo, Japan) with 10× magnification, with a focal depth of approximately 10 μm.[38] Illumination was provided through the microscope in dark-field mode by a continuous cold-light source (ILP-1, Olympus).

The recordings of surface layer removal were analyzed using MATLAB (The Mathworks, Natick, MA, USA), by converting each frame to black and white and determining the cleaned area. The size of each pixel was determined using a calibration grid with markers of well-defined size.

3. Layer deposition

The glass slides on which materials of interest were deposited were made of fused silica wafers. A circular chamber of 8 mm diameter and a depth of 158 μm and four protruding notches that match the notches in the silicon substrate (described before) were etched on one face of each glass slide section. The wafer was then diced in chips with a side of 10 mm. In this way, when placing the glass slide on top of the silicon substrate a microchamber of 100 μm height was formed (see Figure 2). Each material type that was investigated required a different deposition procedure, which is now outlined.

a. Solid hard materials. A single wafer sputter coater (home-made system available in MESA+ Nanolab) for deposition of metallic layers was used to deposit gold, platinum, chromium, and titanium. To deposit organic materials (photoresists Olin 35 and AZ96), hexamethyldisilazane (HMDS) was first spin-coated as a primer to provide chemical bond of the photoresists and strong adhesion to the glass slide on a single wafer spin-coater (Primus coater WB21).

b. Biomaterials. The biofilm model used here was described recently for use in endodontics.[39] In brief, round glass coverslips attached to a customized stainless steel lid were suspended in a medium inoculated with bacteria. In this model, biofilm attachment and growth is an active process against gravity. Microbiology cells of *Enterococcus faecalis* V583 and *Pseudomonas aeruginosa* HG 1776, both clinical isolates, were grown and maintained as pure cultures on blood agar plates. *E. faecalis* was cultured under anaerobic conditions (80% N_2, 10% H_2, and 10% CO_2) whilst *P. aeruginosa* was cultured in air, both at 37 °C. Growth medium for overnight cultures of biofilms was BHI broth containing 0.5 BHI, 50 mmol/l 1,4-piperazinediethanesulfonic acid, buffer, 5% saccharose, and 1 mmol/l Ca^{2+}. Phosphate-buffered saline was used to wash during refreshment of the medium. *E. faecalis* and *P. aeruginosa* were inoculated in wells with additional Ca^{2+} in the broth of a 24-well multiwell plate. Round glass coverslips, diameter 12 mm, and thickness 140 μm, mounted on a custom-made stainless steel lid, were suspended in the broth. In this experiment, biofilms grown for 96 h were used. The broth was refreshed daily. Inoculation of bacteria and the biofilm growth took place at 37 °C in air. The thickness of the biofilm was estimated to be 20 μm, with some bacteria colonies protruding up to 50 μm above the glass substrate.

A biofilm was mimicked with a hydrogel, created by dissolving 1 g gelatin (Merck, Whitehouse Station, NJ, USA), 0.02 g hyaluronan (sodium hyaluronate 95%, Fisher, Waltham, MA, USA), and 0.1 g red food color (KTC, Wednesbury, UK) in 45 ml warm water.[40] Hollow glass spheres with a mean diameter of 10 μm (Sphericel, Potters Industries, South Yorkshire, UK) were added as tracer particles. The final density of the hydrogel was $1.07(\pm 0.07) \cdot 10^3\,\mathrm{kg/m^3}$. This hydrogel was cooled down to room temperature before depositing on a glass slide with raised edges of approximately 100 μm height. The glass slide was then left to cool down for 7 or 15 min, during which the hydrogel dries and attaches to the glass, before the ultrasound and imaging was applied.

MCF-7 human breast carcinoma cells were cultured on the same glass slides; its adhesion resistance when exposed to the cavitation bubbles from the triangular array of micropits was investigated in the cavitation setup. The culture medium was made of Dulbecco's modified eagle medium (DMEM, Gibco®), L-glutatmate, fetal bovine serum (FBS), antibiotics (Penicillin and Stretopmycin), and fungicide.

Table I gives an overview of the various deposited materials and their properties.

TABLE I. Overview of material properties and removal characteristics.

		Contact angle (°)	Removal by. (Y/N/partial)	Removal rate	
Material	Layer thickness (μm)	Advancing, receding	Bubbles, scratch	(mm^2/s)	Adhesion[a]
Glass	…	$79.9\pm1.3, 41.0\pm1.7$	…[d]	…[e]	…[e]
		Solid materials			
Gold	$45 \cdot 10^{-3}$[b]	$86.9\pm0.5, 72.7\pm0.6$	Y, Y	0.01	2260 ± 50 N/m
Platinum	$36 \cdot 10^{-3}$[b]	$87.0\pm0.3, 73.7\pm0.9$	Y, Y	0.001	4400 ± 150 N/m
Chromium	$45 \cdot 10^{-3}$[b]	$75.7\pm0.6, 42.5\pm1.5$	N, N	…[e]	…[c]
Titanium	$15 \cdot 10^{-3}$[b]	$73.6\pm0.8, 45.8\pm2.4$	N, N	…[e]	…[c]
		Organic materials			
Olin	3.5 – 5.2[b]	…[c]	N, P	…[e]	…[c]
AZ96	2.0[b]	…[c]	N, P	…[e]	…[c]
		Biomaterials			
Biofilm	20	…[c]	Y,…[c]	0.1	10^{-1} N/m^2
Hydrogel	100	…[c]	Y,…[c]	0.1	…[c]
Cells	…[c]	…[c]	Y,…[c]	…[c]	…[c]

[a]Solid materials: N/m, measured with AFM; viscoelastic materials: N/m^2, measured with hydrodynamic technique.
[b]Thickness determined with a profile measurement device (Veeco Dektak 8).
[c]These values could not be measured.
[d]No glass erosion took place as a result of bubble cavitation activity for less than 30 min.
[e]Not applicable.

C. Cavitation damage

The glass substrate onto which the gold was deposited was inspected for erosion damage using a scanning electron microscope (SEM, HR-SEM 1550, Zeiss). After the gold was removed by cavitation, the glass substrates were exposed to cavitation for another 1, 5, 10, 15, or 30 min before SEM images were taken.

D. AFM up-thrust measurements of cavitation cloud force

An AFM (Agilent 5100) in non-contact tapping mode was used to measure the up-thrust force from the bubble cloud. A silicon n^+ flat disc tip cantilever (Nanosensors PL2-NCLR-10, spring constant of 48 N/m and resonant frequency 190 kHz in air and 73 kHz in water) with a diameter of ca. 1.8 μm and tip height of ca. 12 μm was used. The cantilever was withdrawn 100 μm from a single-pit substrate surface to mimic the separation between the micropits and "to-be-cleaned" surfaces in the previous measurements. Both low and high ultrasonic powers were used, although for the high power the resulting signal was clipping. The cantilever approached from a distance of 1 mm in a line passing over the bubble clouds. As it happens in the experiments with the glass slides and deposited layers, the bubbles traveled to the cantilever and collapsed against it. Unfortunately, the cantilever was destroyed during the second pass at this force, so the measurements were stopped.

III. RESULTS

A. Cavitation occurrence, in the absence of deposited materials

Switching on the ultrasound leads to a continuous generation of microbubbles with a size range of 2–17 μm, determined from the video recordings and shown in Figure 3 (see also Fernandez *et al.*[41]). Bubbles smaller than 2 μm could not be visualized due to the resolution of the camera. Varying the pressure amplitude (power) and the different arrangements of pits resulted in different bubble patterns, as a result of the complex interplay of primary and secondary *Bjerknes forces*, micro-streaming and also the inertial forces acting on the moving microbubbles in the close vicinity of the glass slide. The bubbles were observed to travel towards the glass slide on top of them where they come in focus of the optical setup. This upward motion is a result of the effect of secondary Bjerkness forces, which makes bubbles close to a hard surface

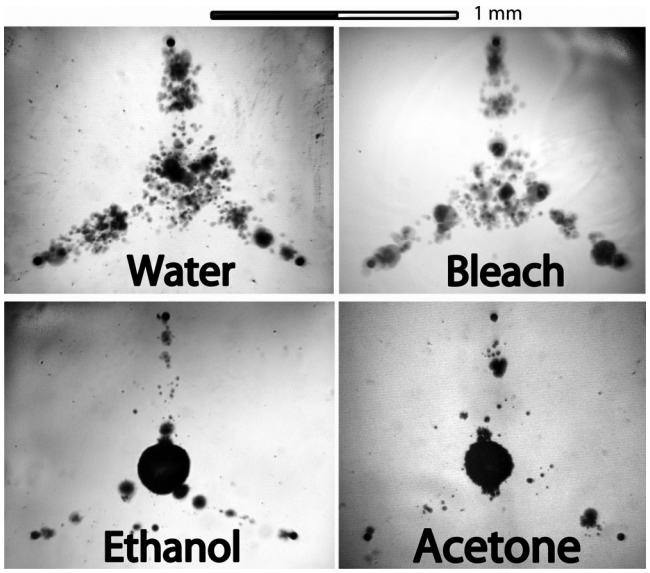

FIG. 3. Bubble pattern for four different liquids tested (no glass slide on top). The bubbles generated are clearly different for each substance but qualitatively similar between water and bleach and between ethanol and acetone.

"feel" the presence of their image bubble as an attraction force, driving the bubbles closer to the wall.

Increasing the power resulted in an increase in the number of ejected bubbles around the pits, forming a bubble cloud or cluster. At high power, with more than one pit, the bubble clusters are attracted to each other and at a given power level (between 0.182 and 0.629 W), the bubbles start to travel towards the geometrical center of the pit array[28,41] (see Figure 4, left column). These bubble cluster configurations are reversible, although there is hysteresis in the amplitude necessary to return to the separated clouds, which is lower than needed for making the bubbles travel to the geometrical center of the pit configuration.

B. Removal of deposited materials by cavitation

1. Observations

Compared to the experiments with and without glass slide, a clear difference can be observed in terms of stabilizing the free water-air interface oscillation when the glass slide is not present. When the glass slide is placed, the traveling and standing wave components change dramatically, contributing to complex effects of bubble cavitation conditions (measured for example through the occurrence of sonochemical reactions).[42]

The opaque materials deposited on the glass slide, when placed on top of the cavitation cell, did not allow for optical visualization of the cavitation bubbles. However, taking as a representative example the case of deposited gold, when switching on the ultrasound at low power (0.182 W), we see that almost instantly (within 2 s) a small opening appears in the gold layer right on top of where the pits are located (see Figure 4). If the power is kept constant the removed gold layer area increases slowly over time. For the case of one pit, increasing the power makes the removed area increase until a maximum area is reached (approximately 0.03 mm^2). Increasing the power for the two, three, and four pit geometries, for which situation the bubbles travel to the geometrical center as described above, an area corresponding to the area of the bubble trajectories is removed. Therefore, for two pits, a linearly extended area is

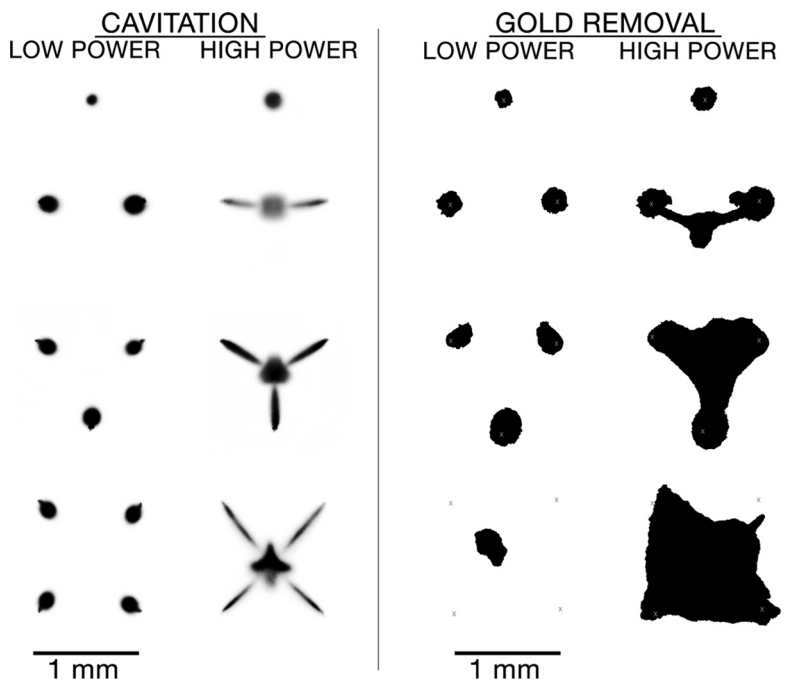

FIG. 4. From top to bottom and left to right, the cases for 1 to 4 pits at low and high power. Left: Bright field illumination (inverted color) showing bubble patterns with slow speed imaging. Right: Contour shape of cleaned area in gold (black) due to bubble cavitation.

typically observed. Accordingly, we find a triangular shape for the three pits and a distorted rectangular shape for the case of four pits; see Figures 2 and 4, right column. For Au and Pt, we observed a similar surface removal behavior.

For the cases of deposited Cr, Ti, and the organic materials, there was no surface removal with the same initial conditions as for Au and Pt. Manually creating a scratch in the layer close to the geometrical center allowed for confirming the presence of the bubbles in the scratched areas, but no material was removed from Cr and Ti layers. After scratching of the photoresist materials the bubbles were able to detach a few pieces of photoresist material only occasionally (Figure 5). The removed pieces of (all) layers could sometimes be trapped by the oscillating bubbles for a relative long period of time (at least more than 30 s if no conditions changed).

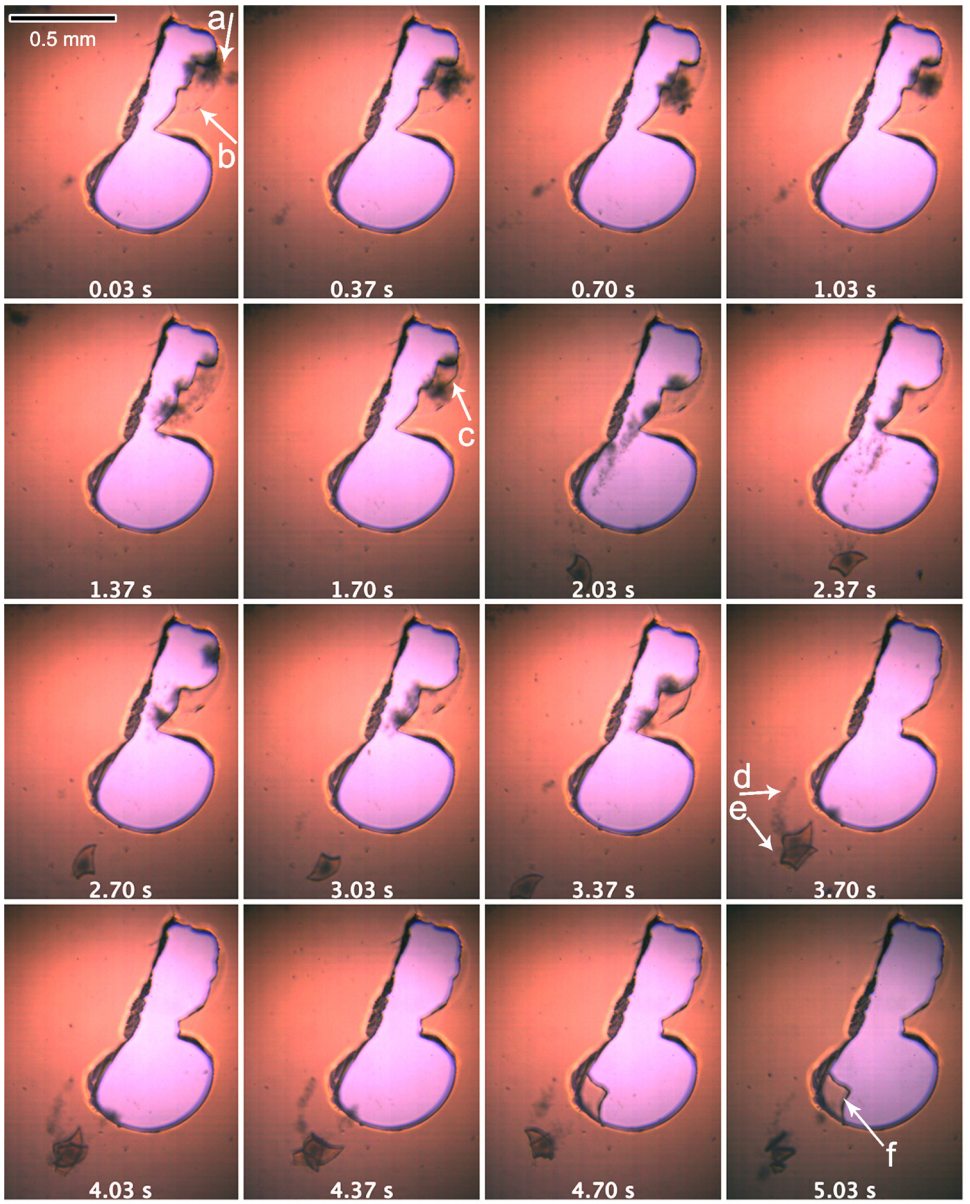

FIG. 5. Montage of a time series of frames recorded for the case of AZ96 photoresist. The center part of each frame shows a portion of manually removed AZ96. Arrow *a* points out a cloud of bubbles as a darker region cavitating close to a crack in the AZ96 layer (arrow *b*). Arrow *c* shows how the crack grew within about 1 s. After 1.7 s, the bubbles (arrow *d*) "trapped" a small portion of AZ96 as indicated by arrow *e*. Eventually, after approximately 4.7 s, the small portion gets stuck in the border line of removed material. The pits do not appear in these pictures since they are out of the field of view (enhanced online) [URL: http://dx.doi.org/10.1063/1.4747166.1].

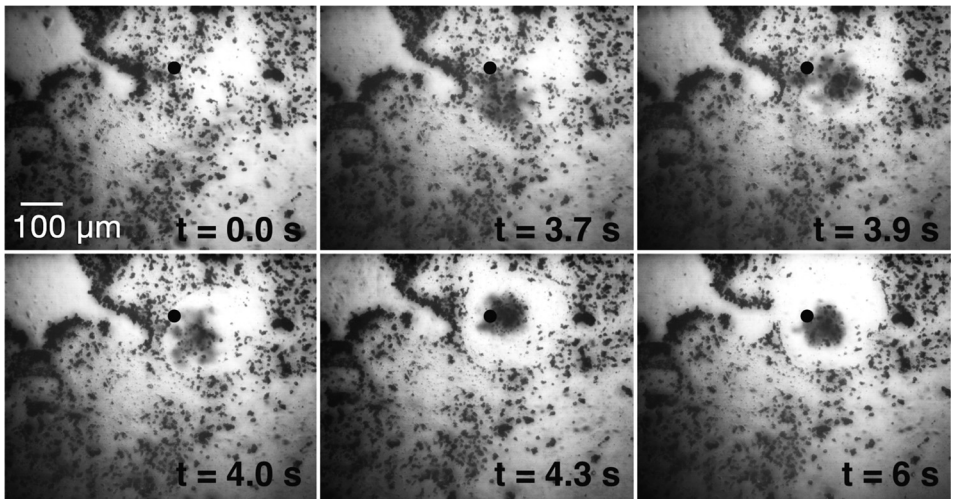

FIG. 6. Stills from a recording of a biofilm being removed by bubbles. The gray area with black dots is the area covered by biofilm, the location of the pit is indicated with a large black dot. The bubbles can be identified as the blurred dark region around the pit (enhanced online) [URL: http://dx.doi.org/10.1063/1.4747166.2].

When the ultrasound is switched off abruptly, the pits may be expected to be filled with water and perhaps, if a bubble is still inside any of the pits, are unable to nucleate more bubbles, deactivating the acoustic bubble generation. If ultrasound is turned on again therefore no cavitation from the micropits takes place. This is why this procedure allows for studying the effect of acoustic streaming alone on material removal. We could not observe removal of any material in the situations where no bubbles were present, allowing us to conclude that the forces associated to streaming alone were not sufficient to remove any of the tested materials. The quantification of streaming from the air-filled pits could not be assessed with the current setup.

The biofilm that was grown on a glass substrate was initially visible as a gray area containing dark clusters of bacteria (Figure 6). Due to transparency of the biofilm, the bubble cloud below the biofilm-covered substrate was visible when the ultrasound was turned on. The biofilm was then removed quickly when the bubble cloud was attracted by the biofilm-covered substrate. No biofilm was removed by the streaming or by bubble clusters when not attracted to the glass surface.

A similar behavior was observed for the hydrogel. The hydrogel appeared softer and attached with weaker force than the biofilm, both after 7 and 15 min of drying, but neither was removed by the acoustic streaming alone.

The distance between the hydrogel or biofilm and the micropits was less well-defined than for the metal and hard organic deposited layers, due to the non-uniform thickness of these layers and flexible (softer) nature. Therefore, the bubbles were less likely to travel toward these layers, which resulted in slow or no increase in removed area after initial removal.

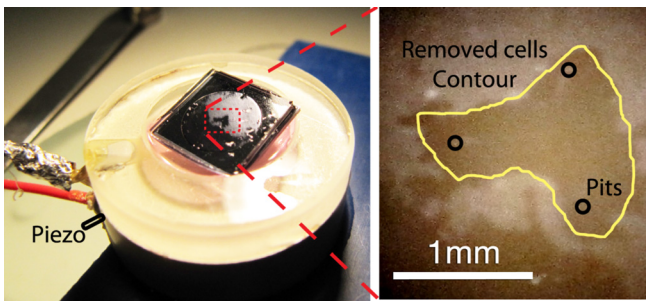

FIG. 7. Cavitation cell and experimental results after removing MCF-7 cells fixed to a glass slide. The liquid cultivation media's pinkish color is visible inside the cavitation cell glued to the piezo.

The MCF-7 cells grown on the glass substrate were also removed when the bubbles were present, leaving the outlier cells attached, as can be seen in Figure 7. The liquid cultivation media produced bubbles similar to those in water. The contour of the removed area resembles again the shape of the bubble cloud for the three pits configuration.

2. Removal rates

The area in which gold has been removed by the bubbles originated from a single pit, after approximately 1 min, is of the order of 0.1 mm^2; for 4 pits this area increases by one order of magnitude to 1 mm^2, see Figure 8. The rate of removal during the initial growth of the removed area is of the order of 0.1 mm^2/s; this reduces by one order of magnitude to 0.01 mm^2/s during steady growth. For platinum, once a scratch had been made, the steady removal rate is of the order of 0.001 mm^2/s.

The removal of the hydrogel and the biofilm were recorded at lower imaging speeds, providing less detailed information on the removal rates. However, estimates for the removal rate of the hydrogel give a value similar to that of gold, being of the order of 0.01 mm^2/s, with initial removal rates up to 0.1 mm^2/s. The initial rate of removal of the biofilm was estimated to be 0.1 mm^2/s as well, with only minor increase in removed area after the initial removal.

The cleaning effect of bubbles is restricted locally by how close the pits and the nucleated bubbles are from the surface to be cleaned. The bubbles cannot travel farther than a given distance away from the pits, or nearby other bubbles. This is due to the required conditions for continuous cavitation such as available gas content and negative pressure values provided by the oscillating pressure field.

C. Different liquids

Bubbles were observed to be generated in all five liquids investigated. Individual images are shown in Figure 3. For water and bleach, the bubble shapes are similar, with an apparent higher number of bubbles than for ethanol and acetone. For these two organic liquids, we can see smaller bubbles ejected from the pits and a larger bubble growing at the midpoint that, upon reaching a given size, floats away. The experiments with MCF-7 cells were carried out with the same liquid cultivation media showing similar bubble cavitation as in water (see Figure 7). We expect similar removal effects for these liquids as for water, but it was not within the scope of this paper to address this topic further.

D. Cavitation erosion

After the maximum period of 30 min of ultrasound exposure, no erosion was visible on the glass surface, as investigated by SEM analysis. This shows a different effect than the erosion

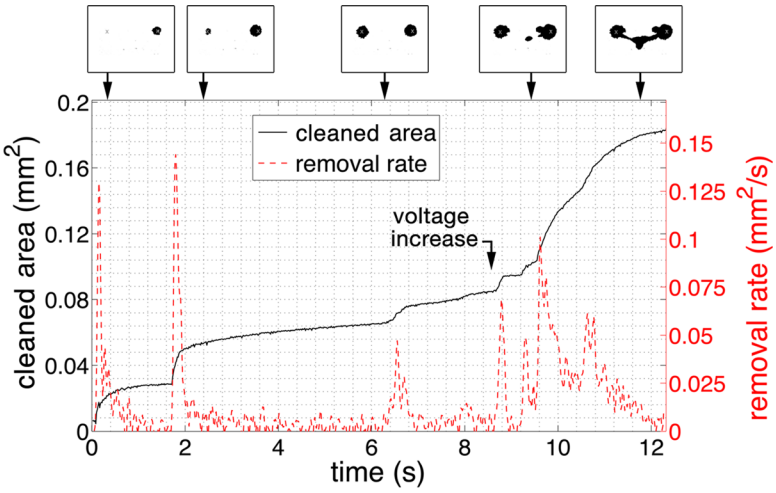

FIG. 8. Size of cleaned area and its derivative (i.e., removal rate) extracted from video measurements (enhanced online) [URL: http://dx.doi.org/10.1063/1.4747166.3].

observed on Si surfaces in our previous studies.[41] The reasons for this are that Si has a crystalline atomic structure and is brittle whereas glass is amorphous and does not exhibit the same mechanical properties.[60] Additionally, the erosion we observed on Si surfaces was on the substrates from which the bubbles were generated, whereas here the bubbles have travelled a considerable distance (150 μm from its nucleation sites) to the glass surface, and the acoustic conditions have changed considerably.

E. Bubble cloud forces

The AFM measurements showed that the force was intermittent, with an average deflection of the cantilever of ca. 500 nm, which corresponds to a force of 20 μN. Using the tip area of the cantilever, the pressure exerted by the bubble cloud can be estimated to be of the order of 50 atm.

The force measurements in both directions of sweep were symmetric, which is especially important for the direction that runs along the length of the cantilever, across the tip, and into free water (where there are no bubbles present). The sweep force had a plateau maximum attributed to the cantilever being directly above the pit, plus slightly to either side but with the bubble streams redirecting to the tip. The value of the force given is the average of the maxima of both the lateral and long ways sweeps, which agree with each other to within error, which thus represents the bubbles hitting the end of the cantilever.

The sweeps pass over the end of the cantilever so we assume that the force measurements can be interpreted in the usual sense in AFM measurements. That the sweep along the length of the cantilever and into free space appears symmetric, represents the fact that the cantilever's "lever" is more than double the distance away from the surface.

Finally, in terms of incorrectly interpreting interference from bubbles as deflection, the laser spot is wholly and exclusively on the back side of the lever (we do not see interference with the bare substrate from an overlapping spot, as an example of the standard control measure). The chip is much wider than the probe's 2 μm end and all bubbles direct towards the end and terminate there for the cases when we use the force measurement.

Also, the temporal resolution limit is given by the resonant frequency (190 kHz in air and 73 kHz in water), which is lower than the piezo frequency (200 kHz), so we measure only averages of impacts and not individual events.

IV. DISCUSSION

A. Cleaning action of bubbles

With the micropits employed in this study, it was shown that metal thin layers (Au and Pt), biomaterials (biofilm, cells, and hydrogel), and organic materials (photoresists) could be removed in a certain local area, defined by the bubble cloud from the micropits. Surprisingly, the removal rates were similar for the metal and the viscoelastic layers, while they all have entirely different mechanical and adhesive properties. This suggests that the bubbles can exert enough mechanical force to remove all of these materials, but that the amount of material that each bubble can remove during one cycle is limited. The deposited material will have to be removed piece by piece, cycle after cycle as a result of several bubbles (clusters) cavitating close to a layer (see Figure 7). As more material gets removed, the bubbles have to travel a larger distance from their origin (pit or geometrical center of the pits array), but are becoming less likely to do so, consequently slowing down the removal rate.

When acoustic cavitation bubbles are in contact with hydrophobic surfaces, it could be expected that no cushion layer of liquid exists that would dampen the liquid jet impact as a result of bubble collapse (the hydrophobic or -philic properties of surfaces and adhesion forces among them have been reported elsewhere).[43–45] Accordingly, the hydrophobicity of the deposited material might have an influence on the material removal, as for bubbles it is easier to collapse towards a hydrophobic wall. As reported elsewhere, the hydrophobic force is uniquely determined by the contact angle.[46] Interestingly, water on Au and on Pt, both removed by the cavitating bubbles, has a much higher (receding) contact angle than on the other metals (see

Appendix D and Table I for contact angle measurement details and results), suggesting that the bubbles could reach those two metals more easily than the other metals. It is not known how much this effect contributes to the cleaning effect.

The fact that microbubbles were generated in ethanol, acetone, bleach, and cell cultivation medium as well as in water suggests that the cleaning with the help of microbubbles can be enhanced for chemical cleaning processes. AZ96 and Olin are commonly removed by acetone; bleach is used routinely in biological/medical applications like dentistry to kill bacteria. According to the results of this study, cavitation could mechanically enhance the chemical removal.

We focused on water since is the "greenest" solvent normally used in cleaning applications but other liquids may be used with similar effects. Another important fact related to our experiment is the small volumes needed to remove the desired substrates. This becomes important when considering cleaning applications with less green solvents (e.g., acetone, toluene, etc.).

To address the influence of the radicals produced by the cavitating microbubbles[28] on the removal of deposited metal materials, all the metals were exposed to hydrogen peroxide (Sigma-Aldrich 30% as provided). For Au, there was no reaction observed at least for the first 5 min, after which occasionally some small regions presented small detachment areas (ca. 1 mm^2). For Pt, there was some chemical activity observed (bubbling and gas formation) that led to detachment of virtually the complete layer in a couple of seconds. For Cr and Ti, there was no reaction within the observation time of 10 min. This allows us to conclude that if there is any contribution of chemical radicals (e.g., $H^{\cdot}$ or $OH^{\cdot}$) to the removal rates it will be minimal under the conditions attained with cavitation bubbles nucleated from the pits.

The acoustic microbubble generation from the micro pits can be sustained for at least several hours if the temperature is kept constant and gas loss is prevented. This means that the loss of gas associated to the microbubble generation does not deactivate the pits, evidencing a process of rectified gas diffusion into the pits. More details on the bubble behavior can be found elsewhere.[28,41]

We observed stable cavitation from the pits with the glass slide placed on top for at least 30 min. However, normally the removed layer areas did not increase much more after the first 3 min if no change in the ultrasound conditions or moving of the glass slide took place.

Additionally, the low operation power compared with conventional ultrasonic cleaning devices (one order of magnitude lower in our case) and the control over the areas to be removed, makes the present cleaning device useful in several applications. Furthermore, the amount of erosion damage of the glass substrate was not possible to detect.

B. Detachment kinetics

1. Solid hard materials

The detachment of material layers by acoustic cavitation bubbles can occur due to material defects, at which the bubbles can perform further detachment. Once a crack is formed, detachment could proceed by peeling and tearing mechanisms due to bubble jetting, and presumably also due to shock waves generated at cavitation bubble collapses and reflections from the hard surfaces. The contribution of streaming can be ruled out based on the above reported observations that there is no cleaning for streaming only (without bubbles). Note that the removal of a thin film may follow a different timeline than traditional cavitation erosion in bulk materials, as the material properties of the bulk and a layer of the same material might be different.[47] To explain the differences in cleaned area and removal rates between the various metals, we have to consider their different adhesion characteristics.

For the *metals*, a first estimation can be obtained by considering the formation of metal oxides on the surface of the metals. Even though the films are sputtered under argon atmosphere conditions, the thickness of all layers is small enough to allow metal oxides to form on the surface. It is known that thin films of oxygen active metals have a higher adhesion to glass than films of noble metals[48] because of molecular electrostatic bonds between the metal oxides and glass.[49]

The likeliness of a metal to form an oxide layer can be obtained from its affinity for oxygen, which is directly related to the (negative) heat of oxide formation of the metal. Au and Pt

(heats of oxide formation of 79.5 kJ/mol and −134 kJ/mol for Au_2O_3 and PtO_2, respectively) do not oxidize easily since these are noble metals, and are therefore expected to have a lower adhesion to glass than Cr and Ti (heats of oxide formation of −1130 kJ/mol and −912.1 kJ/mol for Cr_2O_3 and TiO_2, respectively).[50,51]

The bonding of photoresists (AZ96 and Olin) to glass is strengthened by the strong chemical bond provided by the HMDS priming step. For that reason, only where defects in the layer existed, the bubbles were able to remove material.

The exact value for the adhesion for these solids is difficult to obtain, as the ways and experimental techniques to quantify it are still controversial.[52] At the root of this problem lies the fact that the individual surfaces to be bonded (metal/inorganic layers, and glass surface in our case) have different properties when bonded than when separated. Many factors can affect a bond, such as impurities, roughness, defects, or inhomogeneity on any of both substances, actions of the environmental and mechanical stresses.

Therefore, instead of theoretically predicting the adhesion of the solids of which the layer and substrate are made off, it is more relevant to attempt to measure the actual deposited materials' adhesion with a given experimental system or technique. There are many adhesion measurement techniques described in the literature, including nucleation methods (based on deposition, only able to give basic adhesion values) and mechanical methods (direct pull-off, moment or topple, ultracentrifugal, ultrasonic, adhesive tape peel, scratch, abrasion, laser spallation, etc.).[47] However, the values provided by one technique or given apparatus might not coincide with another technique or with values given in the literature for similar systems. Comparison with the literature should therefore be treated with care, and it is advisable to perform adhesion tests in each individual system.[50]

In order to get a qualitative comparison for the adhesion of the solid hard materials used in this study, we have performed our own scratch tests on the solid hard materials, using an AFM and standard adhesive tape test. The details can be found in Appendices A and B, respectively; the relative adhesion strength of these materials can be summarized as follows: Au < Pt < Olin and Az96 < Ti and Cr.

As another qualitative comparison, and more relevant to ultrasonic cleaning, the removal of the solid hard materials was investigated in a commercial ultrasound bath (Appendix C), showing non-localized removal of Au and Pt under maximum ultrasound conditions, or no removal after 10 min. Taking as an example the case of Au, our technique provided better localized and faster layer removal (compare Figures 2 and 11).

2. Soft biomaterials

Biofilms are known to be able to adhere strongly to a substrate. The initial state of biofilm formation is the adhesion of planktonic bacteria to a substrate, after which the biofilm structure is developed. The bacteria themselves adhere to a substrate due to a multitude of forces, based on both physicochemical and molecular/cellular interactions.[53,54] During its mature state, the biofilm has also been found to increase its adherence through the production of functional amyloids, among others.[30]

Literature reports a wide range of viscoelastic and adhesive properties of encountered biofilms, as these properties depend on the ecology of the biofilm and also on the conditions under which the biofilm has been grown.[29,30,54–56] Furthermore, the properties of the substrate itself are important, for example the surface roughness and hydrophobicity.[30,54]

A *hydrogel* can have better defined viscoelastic properties, as there is more control over its production, and can be used as a substitute for a biofilm when studying the mechanical behavior of biofilms.[57] However, a hydrogel is not grown but deposited onto the glass slide and therefore its attachment to a substrate is expected to be generally weaker than for a biofilm, relying only on physicochemical interactions between glass and hydrogel proteins.[58]

The elastic modulus and adhesion of the hydrogel were estimated using a hydrodynamic technique, of which the details and results are given in Appendix E. The hydrogel was observed to have a weaker attachment to the substrate than the typical values for a biofilm, which is in agreement with our handling observations. However, considering the observation that the

hydrogel did show viscoelastic behavior, it can be considered a soft biofilm. The mechanical properties of the hydrogel can be further tuned by changing its composition and through cross-linking.

The viscoelastic materials were not removed by the acoustic streaming alone, whereas the cavitation cloud could remove them locally within a few seconds. An explanation for this different behavior could be the timescales at which both components react. The pressure magnitude and fluctuations associated with acoustic streaming could be still in the elastic regime of the viscoelastic behavior; the pressure associated with transient bubble dynamics, however, can locally have a high magnitude and fast fluctuation, causing deformations in the viscous regime, and possibly even in the plastic regime.

Many of the MCF-7 cells grown on the glass slide had been detached due to the induced cavitation cloud. However, optical visualization does not give any information on the cells around the area that was cleaned. Those cells might have been lysed through sonoporation, as has been demonstrated by Ohl *et al.*[15] Their method of dead-live staining could provide the information on the viability of the remaining cells.

V. CONCLUSIONS

The localized generation of cavitation from micropits was shown to be able to remove deposited thin metal and organic films and biomaterials on a millimetric scale in less than 1 min. The shape and extent of the cleaned area is related to the number of micropits; the rate of removal was of the order of $0.1\,\mathrm{mm}^2/\mathrm{s}$. Basic adhesion tests provided some insight into the likeliness of a material to be removed.

The low operation power and small volumes of liquid required, together with the limited cavitation erosion damage, make the cleaning device presented here a "green" solution for localized cleaning in many applications.

ACKNOWLEDGMENTS

The authors acknowledge S. Schlautmann from the MCS group, University of Twente for his support in the microfabrication processes, H. A. Visser from the CTW group, University of Twente for lending surface adhesion equipment, and R. de Ruijter from the PCF group, University of Twente, for assistance in the contact angle measurements. The cells were provided and cultured by A. Sridhar and S. le Gac from the BIOS group, University of Twente.

This research was supported by the Technology Foundation STW, Applied Science Division of NWO and the Technology Program of the Ministry of Economic Affairs, The Netherlands.

APPENDIX A: AFM SCRATCH TEST FOR THE ADHESION OF SOLID HARD MATERIALS

1. AFM scratch tests

a. Experimental setup

The adhesion of gold (Au) and platinum (Pt) was determined by scratching these deposited layers using the same AFM as before, but with a different spherical cap tip (Micromasch NSC35, spring constant of 14 N/m, resonant frequency 315 kHz) in contact mode. For these measurements, the surface was scanned continuously over a $20\,\mu\mathrm{m} \times 20\,\mu\mathrm{m}$ areas with the contact force increased gradually every $5\,\mu\mathrm{m}$. Once the metal layer began to tear, the cantilever was lifted and moved elsewhere on the substrate, before the process was repeated. Several repeated measurements were carried out.

b. Results

Only Au and Pt could be removed with this AFM scratch test. The required removal forces were found to be $22.6 \pm 0.5\,\mu\mathrm{N}$ (Au) and $44.0 \pm 1.5\,\mu\mathrm{N}$ (Pt), which, using a removal width of $R = 10\,\mathrm{nm}$, correspond to peeling strengths of $2260 \pm 50\,\mathrm{N/m}$ (Au) and $4400 \pm 150\,\mathrm{N/m}$ (Pt).

The gold and platinum layers delaminated differently to each other. For the gold layer, once the metal had been compromised, it continued to delaminate from the glass substrate even if the contact force was reduced to less than 0.5 μN. However, the platinum delaminated in a stick-slip, patchy fashion, in any case, so lowering the contact force by only a few percent led to no further damage.

Typical scratch patterns are shown in Figure 9. As a guide to the eye, the AFM probe mount is 30 μm wide.

Even at a constant force of 44.0 ± 1.5 μN, the scratch was intermittent. The scratch widths were increased to 90 μm for platinum to better see the effect.

The required forces and peeling strengths for metal removal given above were measured on defect-free areas of the surface. It is interesting to note that the surfaces peeled at much lower applied forces if the AFM probe collided with an optically-sized ($\sim$10 μm) asperity. For the gold, the required force and peeling strength were dramatically reduced to approx. 2.1 μN and 210 N/m, respectively, whilst those for platinum were reduced to approx. 20 μN and 2000 N/m.

APPENDIX B: MACROSCOPIC SCRATCH TEST FOR THE ADHESION OF SOLID HARD MATERIALS

1. Experimental setup

A hardness tester kit (SP0010, Thermimport Quality Control) and a cross-cut adhesion tester kit (CC2000 SP1690, Thermimport Quality Control) were used to analyze the adhesion strength of the solid hard materials. The hardness tester kit consisted of a Tungsten-Carbide tip with 1 mm diameter and a spring with 0-300 g load capacity and can be used to measure the wear (by scratching) or fail resistance of coatings, plastics, etc. The cross-cut adhesion tester kit is based on ISO 2409 Standards and provides a semiquantitative measurement of adhesion. First, perpendicular cuts with parallel blades were performed through the layers, touching the glass slide; afterwards, a dedicated adhesive tape is attached and, when detached, it can remove weakly adhered patches of each layer. According to the amount of removed material, a classification of surface adhesion quality is given with a score between 0 and 5; 0 being the stronger attached where none of the squares is detached after peeling off the tape.

2. Results

The hardness tester is a simple semi-quantitative test for surface hardness in which all materials layers were scratched with 1 g (minimum setting that could be used).

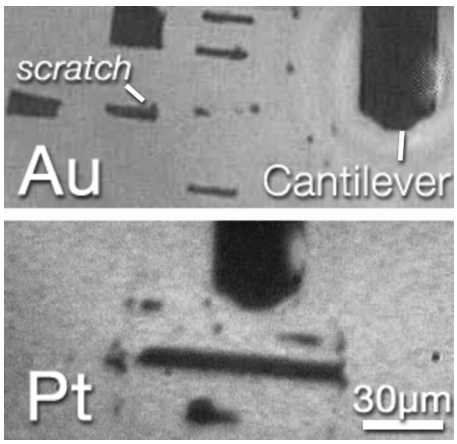

FIG. 9. The top image is for the gold sample and several scratch lines can be seen. Each one is 20 μm wide. The lower image is for the platinum sample.

The scratch test of the different solid hard materials used showed a marked difference between the metal and organic layers (Figure 10). When scratching the organic layers (thicker and more brittle), we observed small parts detaching and it was not possible to cut well defined squares as in the case of the metals.

Au and Pt were the weakest attached materials falling in the 5-and-4 and 4-and-3 category, respectively. For Au layers, we observed that the layer flaked in large ribbons and along the edges where most squares were removed (more than 35% of the total area). For Pt, we saw that most squares were partially or totally removed (more than 15% of the total area). For Cr and Ti, we classified it as 1-and-0 as we observed very small flakes of the coating at the intersections of the cuts and no square could be removed (less than 5% of the area removed).

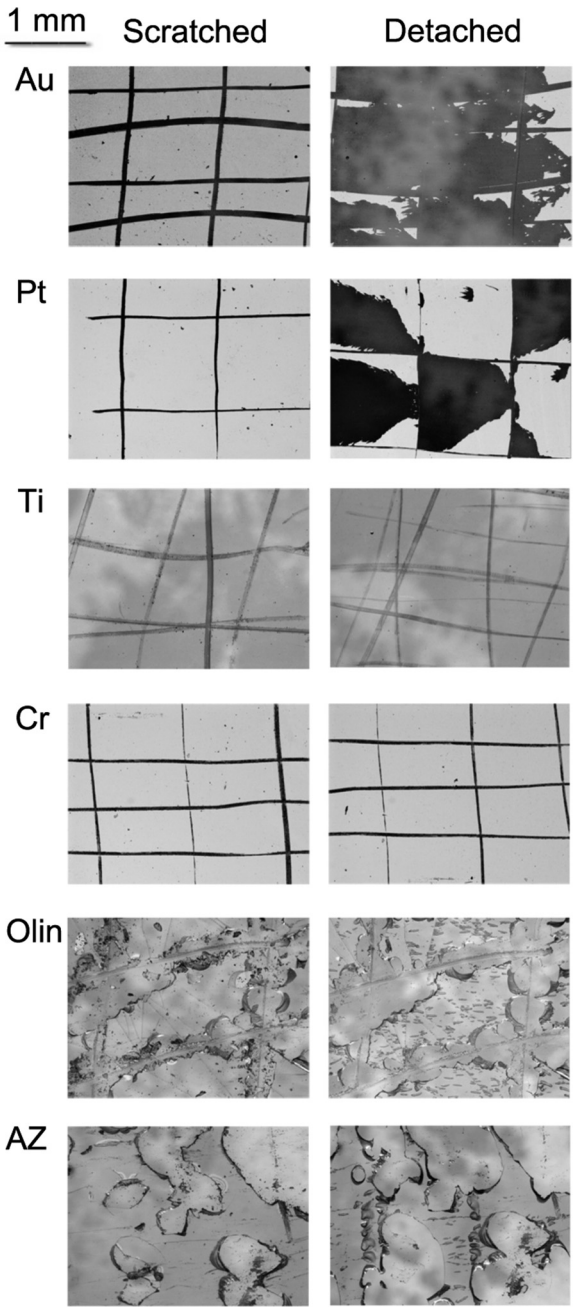

FIG. 10. The left column shows the various deposited layers after the cuts are performed. The right side shows the same region after peeling off the adhesive tape.

For AZ and Olin, we found that some chunks were removed in a way that could be cataloged 2-and-1, but the squares were not neatly formed as these brittle layers cracked; see Figure 10.

Summarizing, the qualitative adhesion of the solid hard materials can be arranged, in order of weakest to strongest, as: Au < Pt < Olin and Az96 < Ti and Cr.

This qualitative quantification is consistent with values provided in the literature using other techniques. For example, for the metals, a laser spallation technique was used to find a direct correlation between the bond strength on silicon oxide substrates with the free energy of oxide formation of the arriving metal vapor for both evaporated and sputtered metals.[59] The energies at which the films detached were: Au (25 J/cm^2), Cr (75 J/cm^2), and Ti (125 J/cm^2), showing the same relative adhesion strength as found in the present study.

APPENDIX C: ULTRASONIC BATH TEST FOR THE ADHESION OF SOLID HARD MATERIALS AND COMPARISON WITH CURRENT SETUP

1. Experimental setup

A commercial ultrasonic bath (VWR) operating at 20 kHz was used to test the adhesion strength of the layers with a conventional ultrasonic apparatus and a comparison of the removal capabilities for each deposited sample was performed.

2. Results

With the ultrasonic bath, no material was removed after 10 min of sonication. All samples were individually placed in a conventional configuration of a glass beaker of 200 ml (Schott) glued to a microscope glass slide (see Figure 11, test A).

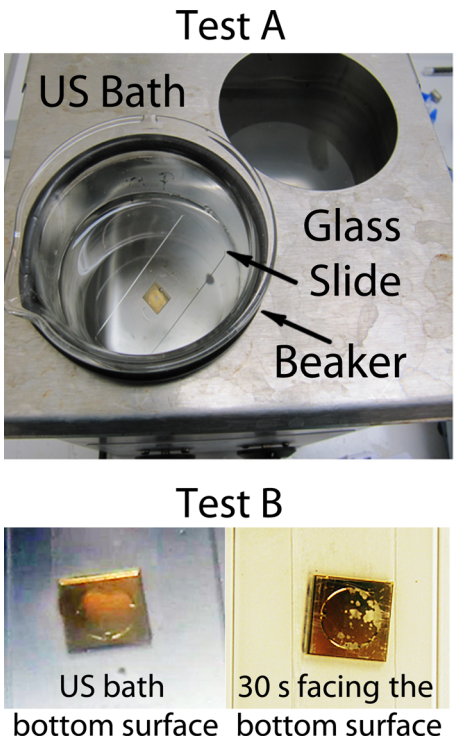

FIG. 11. Experimental conditions provided to test adhesion strength for all layers; in this case for Gold deposited on a glass substrate. Test A shows how the glass substrate was glued to a glass slide and inserted in a glass beaker filled with water as normally cleaning US baths are used. After 10 min, no material was removed in any case. Test B shows the extreme conditions used to be able to remove material (only Au and Ti) but no localization of the removed material.

As an extreme test, we placed each sample facing down, directly against the bottom surface of the ultrasonic bath. For Au and Pt, we observed surface removal without localization and for Cr or Ti we saw no removal at all (see Figure 11, test B).

APPENDIX D: CONTACT ANGLE MEASUREMENT OF SOLID HARD MATERIALS

1. Experimental setup

The advancing and receding contact angles of a sessile drop of tapwater on the gold-, platinum-, chromium-, and titanium-coated glass chips in air was determined using a commercial contact angle goniometer (OCA30, Dataphysics, Filderstadt, Germany). The advancing and receding contact angles were determined automatically thrice by the contact angle goniometer during volume change of a drop of volume 10 μl at a rate of 0.25 μl/s. The non-clean conditions in the ultrasound setup were mimicked by using tap water and by not cleaning the chips before contact angle measurement.

2. Results

The results are presented in Table I. Au and Pt were found to have a larger receding contact angle than the other solid hard materials.

APPENDIX E: HYDRODYNAMIC CHARACTERIZATION OF THE VISCOELASTIC PROPERTIES OF THE HYDROGEL

1. Experimental setup

The properties of the hydrogel used in this study have been measured by determining the strain induced by the stress exerted by the flow from a needle. When the flow through the needle is driven with a positive pressure, a jet is created, which has a stagnation pressure P of $P = \frac{1}{2}\rho u^2$, where ρ is the density of the liquid (water: 1000 kg/m^3) and $u = Q/A$ is the average velocity, estimated from the flow rate Q and the needle orifice A. The setup consisted of a 22 G needle (Terumo, Leuven, Belgium; internal diameter of 0.413 mm) positioned at a distance of 300 μm above the hydrogel-covered surface, through which a flow with flow rates in the range 0.01-1 ml/min were created by a syringe pump (NE1010, New Era Pump Systems, Wantagh, NY, USA). By recording (LM165 camera, Lumenera) the displacement of particles embedded in the hydrogel that appeared to be near the stagnation region of the jet, the Young modulus of the hydrogel can be estimated.

Using the same needle but with a negative pressure, a pulling force is exerted on the hydrogel. Parts of the hydrogel detach (sloughing) from the bulk hydrogel when the suction pressure exceeds the cohesive and adhesive forces of the hydrogel. The suction pressure can be estimated roughly from the Bernoulli pressure along the streamlines of the flow toward the needle orifice.

2. Results

The hydrogel, when subjected to stagnation pressure from a jet generated with a needle, displayed elastic behavior for flow rates higher than 0.01 ml/min, and additional viscous behavior for flow rates higher than 0.1 ml/min. By tracking the displacement of embedded particles in the elastic regime, the Young modulus of the hydrogel was estimated to be of the order of 10^{-1} Pa. When using a negative pressure (suction) through the needle, sloughing was observed to occur for flow rates above 0.2 ml/min, from which the adhesive and cohesive strengths are estimated to be of the order of 10^{-1} Pa.

The mechanical properties of the biofilm could not be determined, because its limited thickness prohibited proper recording of its deformation and the other tests used for the organic

materials and metals are not applicable. However, overall the biofilm appeared to be stiffer and better attached to the substrate than the hydrogel was. This agrees with the typical range of values of the Young's modulus and cohesive and adhesive strengths for biofilms given in literature,[29–32,54–56] which are typically two or three order of magnitude higher than those measured for the hydrogel.

[1]A. Prosperetti, Phys. Fluids **16**, 1852 (2004).
[2]D. Lohse, Phys. Today **56**, 36 (2003).
[3]B. M. Borkent, S. Gekle, A. Prosperetti, and D. Lohse, Phys. Fluids **21**, 102003 (2009).
[4]S. Barnett, G. Ter Haar, M. Ziskin, W. Nyborg, K. Maeda, and J. Bang, Ultrasound Med. Biol. **20**, 205 (1994).
[5]M. Ashokkumar and T. J. Mason, "Sonochemistry," in *Kirk-Othmer Encyclopedia of Chemical Technology* (Wiley, 2000).
[6]J. H. Bang and K. S. Suslick, Adv. Mater. **22**, 1039 (2010).
[7]G. Cravotto and P. Cintas, Chem. Sci. **3**, 295 (2012).
[8]M. P. Brenner, S. Hilgenfeldt, and D. Lohse, Rev. Mod. Phys. **74**, 425 (2002).
[9]Y. T. Didenko and K. S. Suslick, Nature **418**, 394 (2002).
[10]D. Lohse, Nature **434**, 33 (2005).
[11]L. Y. Yeo and J. R. Friend, Biomicrofluidics **3**, 012002 (2009).
[12]P. Marmottant and S. Hilgenfeldt, Nature **423**, 153 (2003).
[13]R. Karshafian, P. D. Bevan, R. Williams, S. Samac, and P. N. Burns, Ultrasound Med. Biol. **35**, 847 (2009).
[14]S. Ohl, E. Klaseboer, and B. Khoo, Phys. Med. Biol. **54**, 6313 (2009).
[15]C. Ohl, M. Arora, R. Ikink, N. De Jong, M. Versluis, M. Delius, and D. Lohse, Biophys. J. **91**, 4285 (2006).
[16]C. Ohl, T. Kurz, R. Geisler, O. Lindau, and W. Lauterborn, Philos. Trans. R. Soc. London, Ser. A **357**, 269 (1999).
[17]H. Lee, A. Homma, E. Tatsumi, and Y. Taenaka, Int. J. Artif. Organs **13**, 17 (2010).
[18]E.-A. Brujan, Med. Eng. Phys. **31**, 742 (2009).
[19]R. Dijkink, S. Le Gac, E. Nijhuis, A. Van den Berg, A. Vermes, A. Poot, and C.-D. Ohl, Phys. Med. Biol. **53**, 375 (2008).
[20]C.-D. Ohl and B. Wolfrum, Biochim. Biophys. Acta **1624**, 131 (2003).
[21]T. Mason, A. Cobley, J. Graves, and D. Morgan, Ultrason. Sonochem. **18**, 226 (2011).
[22]P. Riesz and T. Kondo, J. Free Radic. Biol. Med. **13**, 247 (1992).
[23]A. Cobley, L. Edgar, M. Goosey, R. Kellner, and T. Mason, Circuit World **37**, 15 (2011).
[24]T. Okada, Y. Iwai, S. Hattori, and N. Tanimura, Wear **184**, 231 (1995).
[25]P. Gogate and A. Pandit, Ultrason. Sonochem. **11**, 105 (2004).
[26]M. Arora, C. Ohl, and D. Lohse, J. Acoust. Soc. Am. **121**, 3432 (2007).
[27]N. Bremond, M. Arora, C.-D. Ohl, and D. Lohse, Phys. Rev. Lett. **96**, 224501 (2006).
[28]D. Fernandez Rivas, A. Prosperetti, A. G. Zijlstra, D. Lohse, and H. J. G. E. Gardeniers, Angew. Chem., Int. Ed. **49**, 9699 (2010).
[29]C. Picioreanu, M. Van Loosdrecht, and J. Heijnen, Biotechnol. Bioeng. **72**, 205 (2001).
[30]H.-C. Flemming, J. Wingender, and U. Szewzyk, *Biofilm Highlights*, 1st ed., edited by J. W. Costerton, Springer Series on Biofilms (Springer-Verlag, Berlin, 2011).
[31]P. Stoodley, Z. Lewandowski, J. D. Boyle, and H. M. Lappin-Scott, Biotechnol. Bioeng. **65**, 83 (1999).
[32]P. Stoodley, S. Wilson, R. Cargo, C. Piscitteli, and C. J. Rupp, in *Surfaces in Biomaterials 2001 Symposium Proceedings* (Surfaces in Biomaterials Foundation, Minneapolis, USA, 2001), pp. 189–192.
[33]S. Seltzer, I. B. Bender, J. Smith, I. Freedman, and H. Nazimov, Oral Surg. Oral Med., Oral Pathol. **23**, 500 (1967).
[34]H.-C. Flemming, T. R. Neu, and D. J. Wozniak, J. Bacteriol. **189**, 7945 (2007).
[35]I. Portenier, T. Waltimo, D. Orstavik, and M. Haapasalo, J. Endod. **31**, 380 (2005).
[36]L. Kuznetsova and W. Coakley, Biosens. Bioelectron. **22**, 1567 (2007).
[37]A. Zijlstra, "Acoustic surface cavitation," Ph.D. dissertation (University of Twente, 2011).
[38]C. D. Meinhart, S. T. Wereley, and M. H. B. Gray, Meas. Sci. Technol. **11**, 809 (2000).
[39]S. V. Van der Waal, L. W. M. Van der Sluis, R. A. Özok, R. A. M. Exterkate, P. R. Wesselink, and J. J. De Soet, Int. Endod. J. **44**, 1110 (2011).
[40]A. N. Jatariu-Cadinoiu, M. Popa, S. Curteanu, and C. A. Peptu, J. Biomed. Mater. Res. Part A **98A**, 342 (2011).
[41]D. Fernandez Rivas, L. Stricker, A. G. Zijlstra, H. J. G. E. Gardeniers, D. Lohse, and A. Prosperetti, "Ultrasound artificially nucleated bubbles and their sonochemical radical production," Ultrason. Sonochem. (in press).
[42]D. Fernandez Rivas, M. Ashokkumar, T. Leong, K. Yasui, T. Tuziuti, S. Kentish, D. Lohse, and H. J. G. E. Gardeniers, Ultrason. Sonochem. **19**, 1252–1259 (2012).
[43]J. Israelachvili and R. Pashley, J. Colloid Interface Sci. **98**, 500 (1984).
[44]A. Freitas and M. Sharma, Langmuir **15**, 2466 (1999).
[45]R. Vos, M. Lux, K. Xu, W. Fyen, C. Kenens, T. Conard, P. Mertens, M. Heyns, Z. Hatcher, and M. Hoffman, J. Electrochem. Soc. **148**, G683 (2001).
[46]R.-H. Yoon, D. Flinn, and Y. Rabinovich, J. Colloid Interface Sci. **185**, 363 (1997).
[47]K. Mittal, "Adhesion measurement: Recent progress, unsolved problems, and prospects," in *Adhesive Measurement of Thin Films, Thick Films and Bulk Coatings*, edited by K. Mittal (American Society for Testing and Materials, Philadelphia, 1976), pp. 5–16.
[48]P. Benjamin and C. Weaver, Proc. R. Soc. London, Ser. A **254**, 177 (1960).
[49]D. E. Riemer, IEEE Trans. Compon., Hybrids, Manuf. Technol. **CHMT-8**, 474 (1985).
[50]J. Dini, *Electrodeposition: The Materials Science of Coatings and Substrates* (William Andrew, 1993).
[51]*CRC Handbook of Chemistry and Physics*, 52nd ed., edited by R. Weast (CRC, 1971).
[52]J. Minford, "Durability evaluation of adhesive bonded structures," in *Adhesive Bonding*, edited by L. Lee (Plenum, 1991), Chap. 9, pp. 239–284.

[53]Y. H. An and R. J. Friedman, *Handbook of Bacterial Adhesion*, 1st ed. (Humana, Totowa, NJ, USA, 2000).
[54]W. M. Dunne, Jr., Clin. Microbiol. Rev. **15**, 155 (2002).
[55]S. Bayoudh, A. Othmane, L. Mora, and H. Ben Ouada, Colloids Surf., B **73**, 1 (2009).
[56]P. C. Y. Lau, J. R. Dutcher, T. J. Beveridge, and J. S. Lam, Biophys. J. **96**, 2935 (2009).
[57]C. Mayer, R. Moritz, C. Kirschner, W. Borchard, R. Maibaum, J. Wingender, and H.-C. Flemming, Int. J. Biol. Macromol. **26**, 3 (1999).
[58]G. Sagvolden, I. Giaever, and J. Feder, Langmuir **14**, 5984 (1998).
[59]J. Vossen, "Measurement of film-substrate bond strength by laser spallation," in *Adhesive Measurement of Thin Films, Thick Films and Bulk Coatings*, edited by K. Mittal (American Society for Testing and Materials, Philadelphia, 1976), pp. 122–131.
[60]D. Fernandez Rivas, "Taming acoustic cavitation," Ph.D. dissertation (University of Twente, 2012).